THE JOURNAL OF PHYSICAL CHEMISTRY B

Article

pubs.acs.org/JPCB

Variation of Exciton-Vibrational Coupling in Photosystem II Core Complexes from *Thermosynechococcus elongatus* As Revealed by Single-Molecule Spectroscopy

Sepideh Skandary,[†] Martin Hussels,[†] Alexander Konrad,[†] Thomas Renger,[‡] Frank Müh,[‡] Martin Bommer,[§] Athina Zouni,[§] Alfred J. Meixner,[†] and Marc Brecht*[,†,∥]

[†]IPTC and Lisa+ Center, Universität Tübingen, Tübingen, Germany

[‡]Institut für Theoretische Physik, Johannes Kepler Universität, Linz, Austria

[§]Institut für Biologie, Humboldt Universität zu Berlin, Berlin, Germany

[∥]Zurich University of Applied Science Winterthur (ZHAW), Winterthur, Switzerland

Supporting Information

ABSTRACT: The spectral properties and dynamics of the fluorescence emission of photosystem II core complexes are investigated by single-molecule spectroscopy at 1.6 K. The emission spectra are dominated by sharp zero-phonon lines (ZPLs). The sharp ZPLs are the result of weak to intermediate exciton-vibrational coupling and slow spectral diffusion. For several data sets, it is possible to surpass the effect of spectral diffusion by applying a shifting algorithm. The increased signal-to-noise ratio enables us to determine the exciton-vibrational coupling strength (Huang−Rhys factor) with high precision. The Huang−Rhys factors vary between 0.03 and 0.8. The values of the Huang−Rhys factors show no obvious correlation between coupling strength and wavelength position. From this result, we conclude that electrostatic rather than exchange or dispersive interactions are the main contributors to the exciton-vibrational coupling in this system.

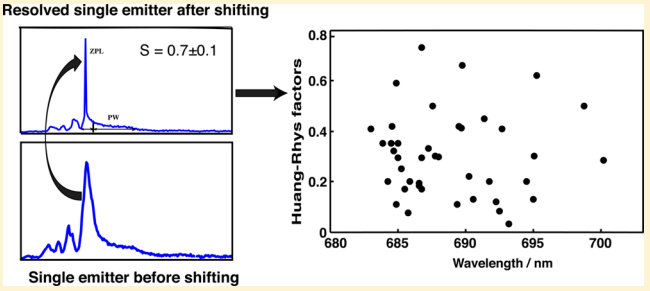

In photosynthetic light-harvesting complexes (also termed antenna proteins), an intricate interplay between different pigment molecules is responsible for light absorption and efficient excitation energy transfer (EET) to the reaction center (RC).[1,2] In oxygenic photosynthesis of cyanobacteria, green algae, and higher plants, the harvested energy is used to oxidize water and reduce plastoquinone in a membrane-embedded pigment−protein complex (PPC) called photosystem II (PSII).[3,4] The functional unit of PSII is a core complex (PSIIcc) that forms dimers (dPSIIcc), which in turn assemble into rows in cyanobacteria[5,6] or are part of a supercomplex with peripheral antennae in higher plants.[7,8] PSIIcc contains, besides the RC, two core antenna subunits referred to as CP43 and CP47 which are responsible for ultimately transferring the excitation energy to the RC, where the charge separation is initiated.[9−12] To understand EET in these systems, it is necessary to know the electronic energy levels of the involved, coupled chlorophyll (Chl) *a* pigments and the interactions of the electronic transitions with vibrational motions of the PPC.[13−15] Important information is obtained from the spectral properties of the fluorescence emitters of the antenna system.[16−18] The fluorescence spectrum of dPSIIcc exhibits a complicated temperature dependence in both plants[18,19] and cyanobacteria.[12,20] Both cases are characterized by a fluorescence maximum at 685 nm at higher temperatures (above 140 K) and the emergence of a second 695 nm fluorescence peak upon cooling down to 77 K. Further cooling reduces the intensity at 695 nm, so that mainly one peak at 685 nm is left at around 4 K. This complex behavior was explained[12] in terms of two distinct pools of Chls, F685 and F695, emitting at different wavelengths and both absorbing at lower wavelengths than the primary electron donor state in the RC. Therefore, these Chls are referred to as red-absorbing or red Chls. Whereas F695 carries the oscillator strength of one Chl, F685 has a larger oscillator strength due to a delocalized exciton state. At 4 K the fluorescence maximum is determined by the state with the higher oscillator strength, i.e., F685. Upon increasing the temperature, EET from F685 to the RC and subsequent quenching by electron transfer sets in and thereby diminishes the fluorescence intensity of this state. Since energy transfer from F695 is frozen out below 77 K, this state is still fully fluorescent and the fluorescence maximum shifts to the red between 4 and 77 K.[12] Note that isolated CP47 complexes do not show such a behavior, since no EET to the RC and subsequent quenching by electron transfer is possible. Instead,

Received: October 22, 2014
Revised: February 20, 2015
Published: February 24, 2015

DOI: 10.1021/jp510631x
J. Phys. Chem. B 2015, 119, 4203−4210

in isolated intact[21] CP47 complexes, the position of the fluorescence maximum was shown[22] to remain constant at 695 nm for $T \leq 75$ K and to move to shorter wavelengths at higher temperatures due to thermal population of higher exciton states.

Besides F685 and F695, a third emitter was identified in plant material, termed F689, that can be detected only in time-resolved fluorescence experiments below 77 K.[23] F685 was assigned to Chls in CP43,[24] whereas F695 was assigned to Chls in CP47.[24−26] Two tentative models assigned F689 to either CP43 or CP47 and left open the possibility that Chls of CP47 contribute to F685.[23] Similar assignments were made on the basis of theoretical studies aimed at the description of a variety of spectroscopic properties of dPSIIcc.[9,12] Reports using excitation-dependent fluorescence line narrowing (FLN)[17] and picosecond time-resolved fluorescence spectroscopy[23] at low temperatures showed inhomogeneous widths of the red chlorophyll bands, where different contributions showed strong overlap. The energy landscape of the CP43 protein was investigated with spectral hole-burning (SHB) and hole-recovery experiments in combination with thermocycling,[27] revealing distribution functions for the barrier heights separating different conformational substates of the protein. So far, these experiments were interpreted by assuming a single value for the Huang−Rhys factor S characterizing the strength of the exciton-vibrational coupling. In the present work, we want to investigate whether not only the electronic transition energy of a protein-bound pigment in PSIIcc but also its coupling to the protein vibrations can vary along the energy landscape of the protein. For Chl *a* in an organic glass and LH2 complexes of purple bacteria, such a variation was reported in combined hole burning, fluorescence line narrowing,[28] and in single molecule spectroscopy (SMS).[29]

SMS is an excellent technique to cope with inhomogeneous spectral widths and reveals subtle spectral details often obscured by averaging over heterogeneous ensembles.[30,31] At room temperature, spectral diffusion and photobleaching hamper the collection of detailed spectroscopic information for most single molecules.[32−35] Lowering the temperature reduces the impact of spectral diffusion,[35−37] and the emission profile of a single emitter composed of a sharp zero-phonon line (ZPL) and a so-called phonon wing (PW) becomes observable.[28,38−40] The ZPL belongs to pure electronic transitions. The PW on the low-energy side of the ZPL belongs to electronic transitions with excitations of vibrational quanta. This coupling is due to the interaction of the chromophore with its surrounding. The ZPL and PW can only be distinguished at low temperatures because of the temperature dependence of the homogeneous lineshape causing the PW to mask the zero-phonon contributions completely at temperatures above 100 K. The ratio between the intensity of the ZPL and PW depends on the strength of exciton-vibrational coupling expressed by the Huang−Rhys factor (S).[41−43] The dimensionless factor S is a measure for the linear exciton-vibrational coupling strength and characterizes the average number of vibrational quanta excited during a particular electronic transition.[44]

Even at low temperatures, the spectral properties of protein bound chromophores depend on time. The time dependence concerns the emission wavelength, intensity, exciton-vibrational coupling, and rate of spectral diffusion.[45,46] The most obvious effect visible in the spectra of single chromophores is spectral diffusion. The fluctuations of the site energy cause spectral jumps extending into the range of several nanometers.[45,46]

The ZPL and PW can be observed in time-dependent spectra series if the rate of spectral diffusion is smaller than the rate of data acquisition, whereas a complete broadening of the ZPLs results if the rate of spectral diffusion surpasses the rate of data acquisition.

In this study, we investigate the spectroscopic properties of dPSIIcc from *Thermosynechoccocus elongatus* at low temperature (1.6 K) at the single-complex level. All recorded fluorescence spectra series consist of sharp ZPLs that cover the whole emission range. We were able to overcome the effect of spectral diffusion for a selected number of lines using a shifting algorithm.[47,48] As a result, the resolved emission profiles of single emitters become visible and the Huang−Rhys factor S can be determined with high accuracy.

MATERIALS AND METHODS

Sample Preparation. Preparation and crystallization of dPSIIcc from *T. elongatus* are described elsewhere.[49] Extensive biochemical characterization of dPSIIcc are summarized in ref 50. For single-molecule spectroscopy redissolved crystals in buffer solution containing 100 mM PIPES (pH 7.0), 5 mM $CaCl_2$, 0.5 M betaine, and 0.03% β-DM showing high oxygen evolution activity were used.[49] The final dPSIIcc concentration was ∼3 pM. For single-molecule experiments less than 1 μL of the sample was sandwiched between two coverslips. Finally, the sample was transferred directly into the cryostat and rapidly plunged into liquid helium. Experiments were carried out using a home-built confocal microscope operating at 1.6 K as described recently.[51] A 665 nm CW diode laser set to 100 μW emission power was used to record spectra series with 100 spectra per data set.

Data Evaluation Process. Two algorithms have been used to evaluate the data sets. Both are implemented using the MATLAB software package. The first algorithm uses smoothing and filtering to detect spectral positions of ZPLs in spectra series and is described in ref 48. By applying it to all data sets a ZPL histogram has been achieved, which is discussed in the Results section.

The second algorithm is useful to overcome the broadening of spectra of single emitters, which are affected by spectral diffusion, for long accumulation times. It works on time-dependent spectra series where the position of the maximum intensity of an emitter is detected in a user-selected wavelength range. Then the single spectra are shifted in a circular manner that the intensity maxima are at the same position. Circular shifting means data points shifted out of the matrix boundaries are moved to the opposite end of the matrix. In the next step the shifted spectra are summed up, giving a spectrum of the single emitter with better signal-to-noise ratio. Finally, a linear baseline correction is applied. To achieve highly resolved single emitter profiles, the shifting wavelength range is selected around the ZPL and the PW, and single spectra showing low intensity or multiple positions of the single emitter are excluded.

To determine the Huang−Rhys factor the intensities of the ZPL, I_{ZPL}, and the PW, I_{PW}, are calculated by numerical integration and the Huang−Rhys factor, S, is obtained by

$$e^{-S} = \frac{I_{ZPL}}{I_{ZPL} + I_{PW}} \quad (1)$$

DOI: 10.1021/jp510631x
J. Phys. Chem. B 2015, 119, 4203−4210

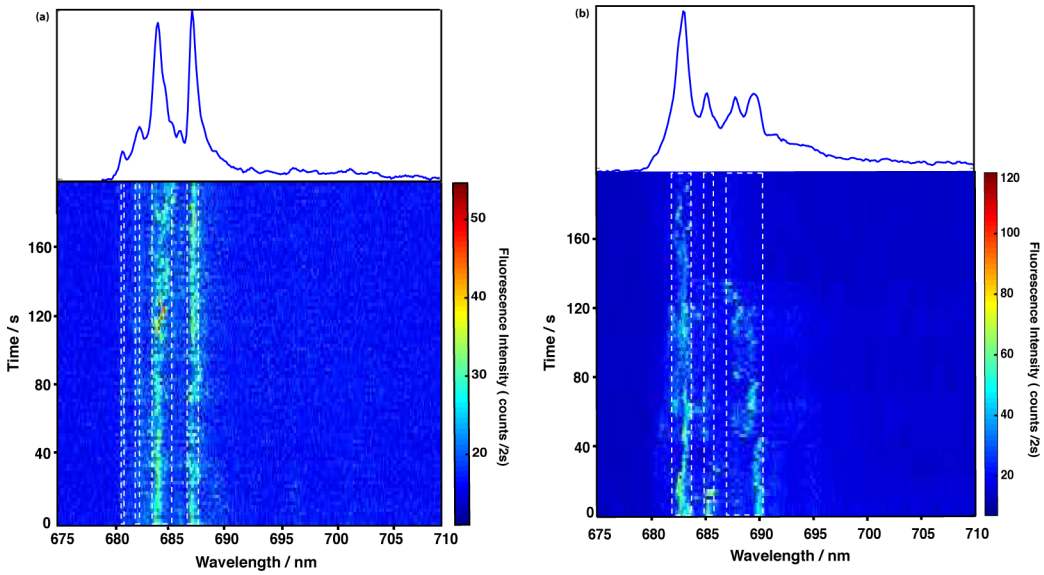

Figure 1. Fluorescence emission spectra of two individual dPSIIcc at low temperature (1.6 K). In both cases, 100 fluorescence emission spectra with an accumulation time of 2 s for each spectrum were recorded subsequently (λ_{exc} = 665 nm). The fluorescence intensity is color-coded (see color code to the right side of each graph). The confined spectral positions of the ZPLs are indicated by the white dashed lines. The average spectrum (on top) is obtained by summation of all spectra in one data set.

RESULTS

Individual dPSIIcc were detected by low temperature confocal microscopy.[20] Figure 1 shows two examples of the time-dependent fluorescence emission of single dPSIIcc. The data set shown in Figure 1a shows four ZPLs. Two sharp and relatively stable ZPLs at 684 and 687.5 nm can be found in the spectra series and the average spectrum, whereas the two weak ZPLs at 681 and 682.4 nm are hardly visible due to their low S/N ratio in time-dependent spectra series. In the data set shown in Figure 1b, one intense ZPL at 683 nm and two weaker ZPLs at 685.4 and 689.3 nm are observable. The first ZPL at 683 nm is relatively stable during the whole series, whereas the two other ZPLs at 685.4 and at 689.3 nm are distorted after 15 and 134 s, respectively. In the mean spectrum on top, the peak at 687.9 nm results from the ZPL which started at 689.3 nm.

ZPLs are clearly visible in all recorded spectra series in the wavelength range from 675 to 710 nm. They show dynamical variations of their spectral position and intensity, but their distribution as well as their time-dependent behavior varies from complex to complex. The variation of each ZPL position is confined to a certain spectral range as indicated by the white dashed lines in Figure 1. The width of this range was determined for clearly distinguishable ZPLs and is 2.5 ± 1.1 nm in the wavelength region from 680 to 705 nm.

The probability of finding a ZPL in a wavelength interval was evaluated for all measured spectra series. For this purpose, the spectral positions of the ZPLs were determined for all data sets by the first algorithm mentioned in the Materials and Methods section. Figure 2 shows the relative occurrence of ZPLs together with the average spectrum calculated for all data taken from single dPSIIcc during this study. The histogram shows the relative distribution of ZPL spectral positions as a function of wavelength between 675 and 710 nm. The ZPLs dominantly occurred in the range between 682 and 687 nm, which corresponds to the peak of the average spectrum with the maximum position at 684.7 nm, and their occurrence decreases at 689 to 701 nm. As it has been discussed in our previous report,[20] the amplitude of the fluorescence from the lowest

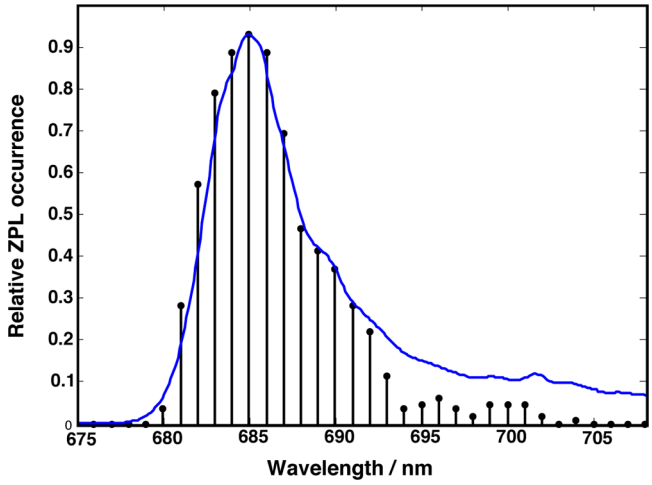

Figure 2. Comparison of the ZPL distribution (histogram) and the average emission spectrum for dPSIIcc. The average spectrum (solid line) represents the sum of all measured (142 data sets) emission spectra from single dPSIIcc at 1.6 K.

emitter F695 in PSIIcc is diminished in our SMS experiments, probably because of the accumulation of triplet states. At low temperatures, a significant part of the excitation is trapped on energetically low-lying antenna chlorophylls because uphill energy transfer to the reaction center is impossible. Because of the longer lifetime of the excited chlorophyll, the yield of fluorescence and triplet formation increases. Carotenoid triplets are formed subsequently by triplet−triplet transfer. The lifetime of Chl triplets decaying by triplet energy transfer to carotene is most likely in the submicrosecond domain.[52]

The determination of the Huang−Rhys factor requires the intensity of the ZPL, I_{ZPL}, and PW, I_{PW}. Determining the position and intensity of ZPLs is straightforward because the whole intensity of a ZPL is emitted within a small spectral range. However, the PWs are less intense and spread over a broader wavelength range than ZPLs. As a consequence,

DOI: 10.1021/jp510631x
J. Phys. Chem. B 2015, 119, 4203−4210

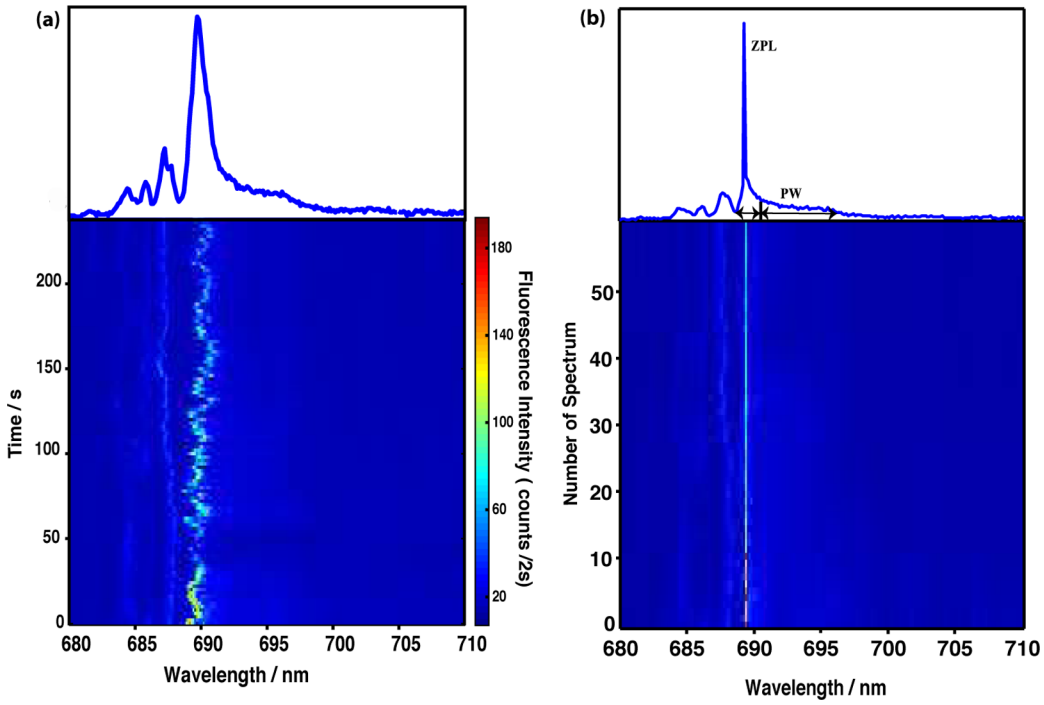

Figure 3. (a) Time-dependent fluorescence emission spectra of an individual dPSIIcc with 2 s time resolution. The average spectrum is given on top. (b) The same data set as (a) after applying the shifting procedure. The bar in the top separates the ZPL and the PW, and the double arrows indicate the spectral range of ZPL and PW. For further details, see the Supporting Information. For the depicted single-emitter profile, we calculated $S = 0.7 \pm 0.1$ with the mean position of ZPL at 689.8 ± 1.2 nm.

determination of PWs is more sensitive to interference with other emitters and background noise; therefore, it is difficult to determine their position and intensity because spectra with good signal-to-noise ratio are needed.

The average spectrum of time-dependent spectra series does not allow us to determine the Huang–Rhys factor because of spectral diffusion leading to multiple peaks and broadening of the spectra as can be seen in Figure 1. It is possible to resolve a ZPL and its accompanying PW if the emission is stable and the background signals can be separated. For this purpose, the position of ZPL is determined for all time-dependent spectra series (see Figure 3). Then all spectra are shifted along the wavelength axis and to one common mean position. After shifting, the background signals are subtracted by applying linear baseline correction.

Figure 3a shows one of the selected time-dependent spectra series with the average spectrum on top. Four ZPLs at 684.5, 685.9, 687.3, and 689.8 nm can be distinguished. However, the only suitable ZPL for applying the shifting algorithm is at 689.8 nm (mean position) because there is no overlap with the other emitters. The wavelength range from 688 to 698 nm was selected for the shifting procedure. Figure 3b shows the series after the shifting, together with the average spectrum (on top). It should be noted that due to shifting along wavelength, the original wavelength scale changed and the time scale converts to number of spectrum. The line at 689.8 nm in Figure 3a changed to a well-resolved line in Figure 3b showing ZPL and pronounced PW with obviously enhanced resolution and signal-to-noise ratio. The signal strength of the individual spectra is too low to resolve the shape of the PW correctly. Using the nicely resolved single ZPL and corresponding PW, we are able to determine the Huang–Rhys factor, *S*. Because of spectral interference of ZPLs and PWs, Huang–Rhys factors are calculated for several estimated borders between positions of ZPLs and PWs, and that is the reason for the relatively large error of the *S* values. For the depicted single-emitter profile, it is $S = 0.7 \pm 0.1$ with the mean position of ZPL at 689.8 ± 1.2 nm.

All data sets were scanned for ZPLs suitable to apply our shifting procedure. Overall, 41 ZPLs were found where *S* could be determined. Figure 4 shows a 2D-scatter plot (*S* versus wavelength) of all 41 ZPLs. The histograms in Figure 4 show the amount of resolved ZPLs according to their wavelength and Huang–Rhys factor values. The distribution of the contribution over the wavelength is in a reasonable agreement with ZPL occurrence in Figure 2. The ZPLs are found in the range of 682–700 nm; the *S* values vary between 0.03 and 0.8. Most of

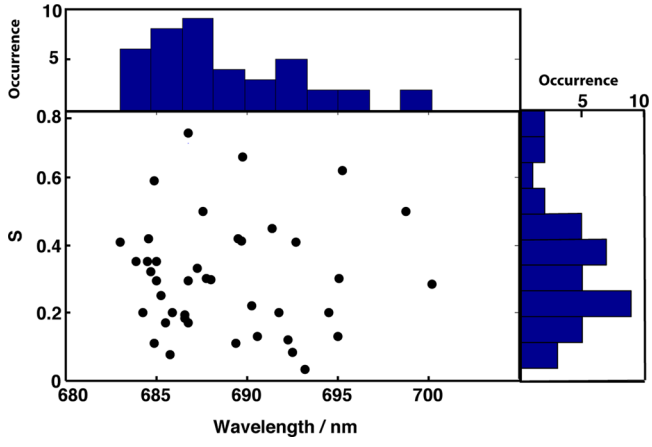

Figure 4. 2D-scatter plot of the wavelength-dependent distribution of the Huang–Rhys factor *S* for dPSIIcc. *S* was determined for 41 resolved emitters in 142 data sets of single dPSIIcc (for more details see text). For both dimensions, histograms are given additionally.

DOI: 10.1021/jp510631x
J. Phys. Chem. B 2015, 119, 4203–4210

the ZPLs occurred at 685 ± 1 nm, and their mean S value is 0.3, in agreement with hole-burning spectra on isolated CP43 complexes, which were analyzed assuming a single S-value.[27,53] Here, we have resolved the distribution of possible S-values of this state. We find a broad range of S-values for F685 as well as for the other emitting states, suggesting that the electron-vibrational coupling varies substantially along the multidimensional energy landscape of the protein. The lowest Huang–Rhys factor of a single dPSIIcc is $S = 0.03 \pm 0.01$ at 693.2 ± 2.1 nm, and the highest is $S = 0.8 \pm 0.1$ at 686.8 ± 0.7 nm (see Figure 4).

In contrast to earlier results obtained for the LH2 antenna of purple bacteria,[29] there is no obvious correlation between S and the ZPL emission wavelength except that the points are somewhat more crowded in the 685 nm region with $S < 0.4$ (Figure 4). One can find quite different values of S for the same ZPL position. For example, at 684.9 nm, we find $S = 0.11$ as well as $S = 0.59$. On the other hand, essentially the same value of S is found for ZPLs at different positions, e.g., $S = 0.35$ at 684.5 ± 1.2 and 683.9 ± 1.1 nm. In the range between 685 and 689 nm, the weakest exciton-vibrational coupling is $S = 0.07$ and the strongest $S = 0.8$. Nearly the same variation of exciton-vibrational coupling is found in the range between 690 and 700 nm with minimally $S = 0.03$ and maximally $S = 0.62$.

DISCUSSION

At 1.6 K the spectra are dominated by sharp ZPLs which are characteristic features of single molecules at low temperature. The ZPLs in the data sets of single dPSIIcc differ in their intensity and spectral positions (see Figure 1).

Multiple lines in different data sets can be the result of (i) spectral diffusion, (ii) static disorder, or (iii) different emitters.[20] (i) Most of the lines which are close to each other can be assigned to single emitters whose site energy changes due to dynamic variations as can be seen in Figure 1. Spectral diffusion is the main reason for variable shapes and positions of ZPLs observable in emission spectra of individual dPSIIcc. Mostly, spectral diffusion leads to time-dependent broadening of the emission (see Figure 1) and not to separated lines. (ii) Chlorophylls bound at the same site might have different transition energies. This includes the possibility that equivalent (symmetry-related) sites in the two dimer halves of dPSIIcc emit at different wavelengths. A Gaussian distribution is often used to describe the extent of static disorder within an ensemble with a fwhm of about 200 cm^{-1},[54] corresponding to about 10 nm wavelength range. (iii) Different low-energy traps corresponding to different Chls in dPSIIcc give rise to separated lines if the low-energy states are not connected to each other by efficient energy transfer leading rapidly to thermal equilibrium.

Stable ZPLs with small discrete jumps are observed (see Figure 1a) if the rate of spectral diffusion is in the range of the experimental accumulation time or slower (slow spectral diffusion). On the other hand, only broadened lines are visible if the rate of spectral diffusion is faster than the rate of data acquisition (fast spectral diffusion).[55]

Our shifting algorithm aims at a correction of the spectra for the effects of spectral diffusion to facilitate the determination of S. Clearly, the algorithm can only correct for the resolvable slow spectral diffusion, while the shifted spectra remain broadened by fast spectral diffusion. Nonetheless, by applying this procedure, we were able to determine the line shapes and Huang–Rhys factors for 41 individual emitters with high accuracy based on 142 recorded data sets.

Earlier analyses of bulk spectra suggest the presence of at least three different emitting entities, F685, F689, and F695,[9,12,23−26] corresponding to three different low-energy traps in dPSIIcc. This suggestion is supported by the present data; i.e., the ZPLs are distributed over a large wavelength range that can be divided roughly into three regions around 685, 689, and 695 nm, which might correspond to F685, F689, and F695, respectively. However, a clear-cut assignment of ZPLs to energy traps is not possible. An assignment would be facilitated by a correlation between ZPL position and S, but no such correlation is observed. There is merely a crowding of data points in the lower left corner of the scattering plot (Figure 4), suggesting that pigments contributing to F685 have preferentially a weak exciton-vibrational coupling (i.e., $S < 0.4$). This result is in agreement with hole-burning studies of isolated CP43 assigning $S \approx 0.3$ to the so-called A-state of CP43,[27,53] which likely corresponds (or at least contributes) to F685.[9]

The red-most state in dPSIIcc, i.e., F695, is assigned to the low-energy trap in CP47. This is proposed[9,10] to be due to Chl29 (in the nomenclature of Loll et al.[56]), but there are other assignments.[57] Hole-burning studies on isolated CP47 suggest this trap to have a relatively strong exciton-vibrational coupling with $S \approx 1.0$.[21] This is only partly in agreement with our results, since all our emitters, including those at low energies, where F695 is expected, have smaller S values. Hence, we have to conclude that we only see a nonrepresentative selection of ZPLs for the state F695 in our single-molecule experiments. As has been discussed in our previous publication,[20] the selection may occur due to the high excitation rate necessary for SMS. Triplet states could be accumulated at the low-energy state F695 of CP47, which, therefore, fluoresces less. It is expected that the Chl triplet states accumulating at F695 are quenched by nearby carotenoids to prevent photodamage that can occur if the triplet state of Chl is reacting with triplet oxygen to form the poisonous singlet oxygen. Of course, we cannot entirely exclude that such or other type of photodamage occurs. In this case, our interpretation of the data relies on the assumption that the photodamage stays local and, therefore, has no influence on the Huang–Rhys factors of the other low-energy sites, which is reasonable. It is an open question why the remaining emitters of F695 exhibit a weaker electron-vibrational coupling than the ensemble on average. It seems that the states with higher exciton-vibrational coupling can more easily undergo an intersystem crossing to the triplet state, probably because the excess energy can be better dissipated by the protein environment during the transition. Finally, we note that also the low-energy emitting states show a random variation of S values.

In contrast to the present data, positive correlations between the wavelength of the ZPL position and the Huang–Rhys factor were reported for the LH2 antenna of purple bacteria[29] and for Chl a in a glassy matrix of 1-propanol.[28] The question arises: Under which circumstances is there a correlation between the solvatochromic shift (i.e., the environment-induced shift of the ZPL position) of the transition energy of a pigment and the strength of the dynamic modulation of this transition energy by environmental vibrations (represented by S)? In the case of LH2, most likely the mixing between exciton states and interchromophore charge transfer (CT) states is responsible for the red-shift as well as for the enhanced electron-vibrational coupling. If the CT state is energetically

DOI: 10.1021/jp510631x
J. Phys. Chem. B 2015, 119, 4203−4210

above the exciton state, this mixing leads to a red-shift of the exciton state. The CT state borrows some oscillator strength from the exciton state, and the exciton state borrows some electron-vibrational coupling strength from the CT state.[58] Note that a CT state, due to its polar nature, exhibits a very strong electron-vibrational coupling.

In the case of Chl *a* in the organic glass, electrostatic as well as dispersive interactions are responsible for the electrochromic shift. Whereas the dispersive interaction, due to the higher polarizability of the excited state (with respect to the ground state) of the chromophore, leads to a red-shift of the transition energy, the electrostatic interaction can lead to both blue- and red-shifts.

As a general rule we expect a positive correlation between the red-shift and the Huang–Rhys factor, if a decrease in the distance between the chromophore and the environmental atoms (leading to an increase in the fluctuation of the transition energy) leads to a red-shift in the transition energy of the chromophore. In the case of the LH2 such a decrease in distance leads to an increase in wave function overlap and thereby to an increase in quantum-mechanic mixing between the exciton states and the CT state. In the case of Chl *a* in the organic glass, a decrease in distance leads to an increase in the dispersive interaction causing an electrochromic red-shift and/or an increase of the absolute magnitude of the electrostatic interaction, which may cause both a red- and blue-shift.

The latter aspect becomes important in proteins. As electrostatic calculations of static site energies and spectral densities of the dynamic pigment–protein coupling show, an electrochromic red-shift in general does not correlate with the Huang–Rhys factor, that is, the integral over the spectral density of the site energy fluctuations.[14,15] In principle, all scenarios are possible: anticorrelation, correlation, and no correlation. Since the electrostatic site energy shifts contain contributions of different signs, depending on the relative position of the charge density of the protein in the difference potential between excited and ground state of the chromophore, the different contributions may partially compensate each other in the static site energy. In contrast, if the charge density is varied in a correlated way (e.g., due to normal mode vibrations of the pigment–protein complex), one could well imagine that the different contributions add constructively in the dynamic modulation of the transition energy.

We, therefore, conclude that for the present system electrostatic interactions are responsible for the static and dynamic shifts of the transition energies of the low-energy exciton states.

The large scattering of the Huang–Rhys factor indicates that the respective Chls are exposed to a certain amount of variability in the interaction with their close surrounding. A measure to determine the flexibility of parts of a protein in the X-ray structure is given by the crystallographic *B*-factors. Figure 5 shows the *B*-factors of dPSIIcc. Chls 11, 48, and 49 show the largest *B*-factors in PSII (using the nomenclature of Loll et al.[56]). Among the Chls showing an increased *B*-factor is Chl29 of CP47. Chl29 seems to be responsible for the emission at 695 nm,[9,11,12,60] and Chl11 also is supposed to be red-shifted significantly.[9,12] Other studies assign Chl26 as the mostly red-shifted.[57] In the case of CP43, pigments with large red-shifts were proposed to be Chls 37, 43, and 45[9,12,61] or Chls 37 and 44.[62] There seems to be no correlation between these red-shifts and an increased *B*-factor. Irrespective of the preliminary character of these assignments, this seems to indicate that there

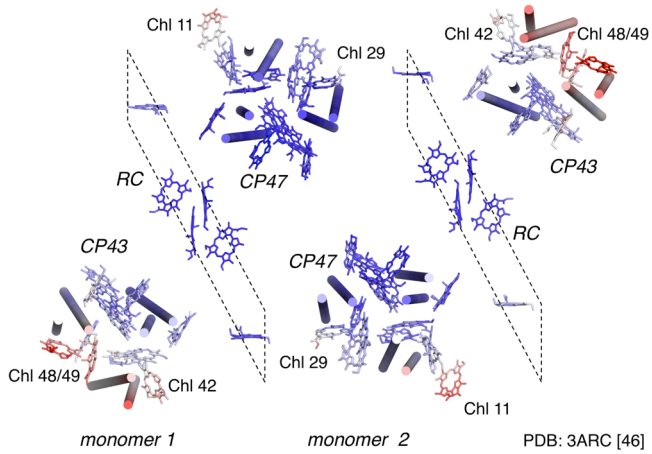

Figure 5. Distribution of the Debye–Waller factor (*B*-factor) for the Chl *a* in X-ray structure of dPSIIcc (PDB: 3ARC).[59] The averaged *B*-factors vary between 20 (colored deep blue) and 50 (deep red). Blue color indicates a small *B*-factor, and red indicates a high *B*-factor. Chl *a* molecules at the outer rim of dPSIIcc show an increased *B*-factor; one is Chl29 of CP47.

is no correlation between red-shift and Huang–Rhys factor, in agreement with our results.

Weak exciton-vibrational coupling strengths as observed here are common for photosynthetic antenna complexes.[63,64] Our SMS study gives uniquely detailed information on the exciton-vibrational coupling where it allows us to determine the Huang–Rhys factor accurately through the homogeneous broadened spectra, whereas SHB and FLN were so far interpreted by assuming a single *S*-value.[28,65,66]

It is encouraging to see that our average *S*-value for F685 ($S = 0.3$) agrees with the *S*-value inferred from SHB experiments on CP43 complexes,[27,53] where F685 is supposed to be located.[9,12] The underlying large variations of the individual *S*-values ($0.1 < S < 0.6$) for this state clearly show that the exciton-vibrational coupling of protein-bound pigments in PSII can vary substantially along the energy landscape of the protein. This result has implications also for the calculation of EET. So far, *S* was assumed to be constant, since no detailed information was available for PSII. In future calculations, it will be interesting to see how the energy transfer changes if a distribution of *S*-values is taken into account.

CONCLUSION

In summary, we have found that the electron-vibrational coupling of protein-bound pigments with low excitation energies in PSIIcc varies substantially. This conclusion can be drawn irrespectively of the accumulation of triplet states, which likely occurs under our experimental conditions and causes the mostly red-shifted emitters to be underrepresented. An implicit assumption in our analysis is that the presence of triplet states does not affect the variations of Huang–Rhys factors. Since these variations are not correlated with the emission wavelength, we conclude that electrostatic interactions are the main contributor to the electron-vibrational coupling in this system.

ASSOCIATED CONTENT

Supporting Information

Description of the algorithm to calculate *S* and the error in the evaluation of the *S*-factors are explained in detail. This material is available free of charge via the Internet at http://pubs.acs.org.

DOI: 10.1021/jp510631x
J. Phys. Chem. B 2015, 119, 4203–4210

AUTHOR INFORMATION

Corresponding Author

*Phone +49-7071-29-76239; Fax +49-7071-29-5490; e-mail marc.brecht@uni-tuebingen.de (M.B.).

Notes

The authors declare no competing financial interest.

ACKNOWLEDGMENTS

This work was supported by the Heisenberg-Program of the Deutsche Forschungsgemeinschaft DFG (BR 4102/1-1 and BR 4102/2-1), by the DFG within the framework of the cluster of excellence on unifying Concepts in catalysis (UniCat), project B1, coordinated by the TU Berlin, Sfb 1078, project A5 (A.Z.), HFSP RGP0063/2013, and by the Austrian Science Fund (FWF), project P24774-N27 (T.R.).

REFERENCES

(1) van Grondelle, R.; Novoderezhkin, V. I. Energy transfer in photosynthesis: experimental insights and quantitative models. *Phys. Chem. Chem. Phys.* **2006**, *8*, 793−807.

(2) Scholes, G. D.; Fleming, G. R.; Olaya-Castro, A.; van Grondelle, R. Lessons from nature about solar light harvesting. *Nat. Chem.* **2011**, *3*, 763−774.

(3) Müh, F.; Zouni, A. Light-induced water oxidation in photosystem II. *Front. Biosci.* **2011**, *16*, 3072−3132.

(4) Müh, F.; Zouni, A. Light-induced quinone reduction in photosystem II. *Biochim. Biophys. Acta* **2012**, *1817*, 44−65.

(5) Mörschel, E.; Schatz, G. H. Correlation of photosystem II complexes with exoplasmatic freeze-fracture particles of thylakoids of the cyanobacterium *Synechococcus-sp*. *Planta* **1987**, *172*, 145−154.

(6) Folea, I. M.; Zhang, P.; Aro, E.-M.; Boekema, E. J. Domain organization of photosystem II in membranes of the cyanobacterium *Synechocystis* PCC6803 investigated by electron microscopy. *FEBS Lett.* **2008**, *582*, 1749−1754.

(7) Dekker, J. P.; Boekema, E. J. Supramolecular organization of thylakoid membrane proteins in green plants. *Biochim. Biophys. Acta* **2005**, *1706*, 12−39.

(8) Caffarri, S.; Kouril, R.; Kereiche, S.; Boekema, E. J.; Croce, R. Functional architecture of higher plant photosystem II supercomplexes. *EMBO J.* **2009**, *28*, 3052−3063.

(9) Raszewski, G.; Renger, T. Light harvesting in photosystem II core complexes is limited by the transfer to the trap: can the core complex turn into a photoprotective mode? *J. Am. Chem. Soc.* **2008**, *130*, 4431−4446.

(10) Müh, F.; Renger, T.; Zouni, A. Crystal structure of cyanobacterial photosystem II at 3.0Å resolution: a closer look at the antenna system and the small membrane-intrinsic subunits. *Plant Physiol. Biochem.* **2008**, *46*, 238−264.

(11) Renger, T.; Schlodder, E. Optical properties, excitation energy and primary charge transfer in photosystem II: theory meets experiment. *J. Photochem. Photobiol., B* **2011**, *104*, 126−141.

(12) Shibata, Y.; Nishi, S.; Kawakami, K.; Shen, J. R.; Renger, T. Photosystem II does not possess a simple excitation energy funnel: time-resolved fluorescence spectroscopy meets theory. *J. Am. Chem. Soc.* **2013**, *135*, 6903−6914.

(13) Renger, T.; Marcus, R. A. On the relation of protein dynamics and exciton relaxation in pigment-protein complexes: an estimation of the spectral density and a theory for the calculation of optical spectra. *J. Chem. Phys.* **2002**, *116*, 9997−10019.

(14) Renger, T.; Klinger, A.; Steinecker, F.; Schmidt am Busch, M.; Numata, J.; Müh, F. Normal mode analysis of the spectral density of the Fenna-Matthews-Olson light-harvesting protein: how the protein dissipates the excess energy of excitons. *J. Phys. Chem. B* **2012**, *116*, 14565−14580.

(15) Renger, T.; Müh, F. Understanding photosynthetic light-harvesting: a bottom up theoretical approach. *Phys. Chem. Chem. Phys.* **2013**, *15*, 3348−3371.

(16) Groot, M. L.; Peterman, E. J. G.; van Stokkum, I. H. M.; Dekker, J. P.; van Grondelle, R. Triplet and fluorescing states of the CP47 antenna complex of photosystem II studied as a function of temperature. *Biophys. J.* **1995**, *68*, 281−290.

(17) Groot, M. L.; Frese, R. N.; de Weerd, F. L.; Bromek, K.; Pettersson, A.; Peterman, E. J. G.; van Stokkum, I. H. M.; van Grondelle, R.; Dekker, J. P. Spectroscopic properties of the CP43 core antenna protein of photosystem II. *Biophys. J.* **1999**, *77*, 3328−3340.

(18) Krausz, E.; Hughes, J. L.; Smith, P. J.; Pace, R. J.; Arsköld, S. P. Assignment of the low-temperature fluorescence in oxygen-evolving photosystem II. *Photosynth. Res.* **2005**, *84*, 193−199.

(19) Andrizhiyevskaya, E. G.; Chojnicka, A.; Bautista, J. A.; Diner, B. A.; van Grondelle, R.; Dekker, J. P. Origin of the F685 and F695 fluorescence in photosystem II. *Photosynth. Res.* **2005**, *84*, 173−180.

(20) Brecht, M.; Skandary, S.; Hellmich, J.; Glöckner, C.; Konrad, A.; Hussels, M.; Meixner, A.; Zouni, A.; Schlodder, E. Spectroscopic properties of photosystem II core complexes from *Thermosynechococcus elongatus* revealed by single-molecule experiments. *Biochim. Biophys. Acta* **2014**, *1837*, 773−781.

(21) Neupane, B.; Dang, N. C.; Acharya, K.; Reppert, M.; Zazubovich, V.; Picorel, R.; Seibert, M.; Jankowiak, R. Insight into the electronic structure of the CP47 antenna protein complex of photosystem II: hole burning and fluorescence study. *J. Am. Chem. Soc.* **2010**, *132*, 4214−4229.

(22) Acharya, K.; Neupane, B.; Reppert, M.; Feng, X.; Jankowiak, R. On the unusual temperature-dependent emission of the CP47 antenna protein complex of photosystem II. *J. Phys. Chem. Lett.* **2010**, *1*, 2310−2315.

(23) Komura, M.; Shibata, Y.; Itoh, S. A new fluorescence band F689 in photosystem II revealed by picosecond analysis at 4−77 K: function of two terminal energy sinks F689 and F695 in PSII. *Biochim. Biophys. Acta* **2006**, *1757*, 1657−1668.

(24) van Dorssen, R.; Breton, J.; Plijter, J.; Satoh, K.; van Gorkom, H.; Amesz, J. Spectroscopic properties of the reaction center and of the 47 kDa chlorophyll protein of photosystem II. *Biochim. Biophys. Acta* **1987**, *893*, 267−274.

(25) van Dorssen, R.; Plijter, J.; Dekker, J.; den Ouden, A.; Amesz, J.; Gorkom, H. Spectroscopic properties of chloroplast grana membranes and of the core of photosystem II. *Biochim. Biophys. Acta* **1987**, *890*, 134−143.

(26) Dekker, J. P.; Hassoldt, A.; Pettersson, A.; van Roon, H.; Groot, M. L.; van Grondelle, R. On the nature of the F695 and F685 emission of photosystem II. In *Photosynthesis: From Light to Biosphere*; Mathis, P., Ed.; Kluwer Academic Publishers: Dordrecht, The Netherlands, 1995; Vol. *1*, pp 53−56.

(27) Najafi, M.; Herascu, N.; Seibert, M.; Picorel, R.; Jankowiak, R.; Zazubovich, V. Spectral hole-burning, recovery and thermocycling in chlorophyll-protein complexes: distribution of barriers on the protein energy landscape. *J. Phys. Chem. B* **2012**, *116*, 11780−11790.

(28) Rätsep, M.; Pajusalu, M.; Freiberg, A. Wavelength-dependent electron-phonon coupling in impurity glasses. *Chem. Phys. Lett.* **2009**, *479*, 140−143.

(29) Kunz, R.; Timpmann, K.; Southall, J.; Cogdell, R. J.; Freiberg, A.; Köhler, J. Exciton self trapping in photosynthetic pigment-protein complexes studied by single-molecule spectroscopy. *J. Phys. Chem. B* **2012**, *116*, 11017−11023.

(30) van Oijen, A. M.; Ketelaars, M.; Köhler, J.; Aartsma, T. J.; Schmidt, J. Unraveling the electronic structure of individual photosynthetic pigment-protein complexes. *Science* **1999**, *285*, 400−402.

(31) Tamarat, P.; Maali, A.; Lounis, B.; Orrit, M. Ten years of single-molecule spectroscopy. *J. Phys. Chem. A* **2000**, *104*, 1−16.

(32) Lu, H. P.; Xie, X. S. Single-molecule spectral fluctuations at room temperature. *Nature* **1997**, *385*, 143−146.

(33) Rutkauskas, D.; Novoderezhkin, V. I.; Cogdell, R. J.; van Grondelle, R. Fluorescence spectroscopy of conformational changes of single LH2 complexes. *Biophys. J.* **2005**, *88*, 422−435.

(34) Schleifenbaum, F.; Blum, C.; Subramaniam, V.; Meixner, A. J. Single-molecule spectral dynamics at room temperature. *Mol. Phys.* **2009**, *107*, 1923−1942.

DOI: 10.1021/jp510631x
J. Phys. Chem. B 2015, 119, 4203−4210

(35) Berlin, Y.; Burin, A.; Friedrich, J.; Köhler, J. Low temperature spectroscopy of proteins. part II: experiments with single protein complexes. *Phys. Life Rev.* **2007**, *4*, 64−89.
(36) Shibata, Y.; Ishikawa, H.; Takahashi, S.; Morishima, I. Time-resolved hole-burning study on myoglobin: fluctuation of restricted water within distal pocket. *Biophys. J.* **2001**, *80*, 1013−1023.
(37) Hofmann, C.; Ketelaars, M.; Matsushita, M.; Michel, H.; Aartsma, T. J.; Köhler, J. Single-molecule study of the electronic couplings in a circular array of molecules: light-harvesting-2 complex from *Rhodospirillum molischianum*. *Phys. Rev. Lett.* **2003**, *90*, 013004.
(38) Huang, K.; Rhys, A. Theory of light absorption and non-radiative transitions in F-centres. *Proc. R. Soc. London, A* **1950**, *204*, 406−423.
(39) Pullerits, T.; Monshouwer, R.; van Mourik, F.; van Grondelle, R. Temperature-dependence of electron-vibronic spectra of photosynthetic systems-computer-simulations and comparison with experiment. *Chem. Phys.* **1995**, *194*, 395−407.
(40) Renge, I. Impurity spectroscopy in glasses and disordered crystals: inhomogeneous broadening and electron phonon coupling. *J. Lumin.* **2008**, *128*, 413−420.
(41) Rebane, K. K. *Impurity Spectra of Solids*; Plenum: New York, 1970.
(42) Personov, R. I. In *Spectroscopy and Excitation Dynamics of Condensed Molecular Systems*; Agranovich, V. M., Hochstrasser, R. M., Eds.; North Holland: Amsterdam, 1983; Chapter 10.
(43) Peterman, E. J. G.; Pullerits, T.; Grondelle, R.; Amerongen, H. Electron-phonon coupling and vibronic fine structure of light-harvesting complex II of green plants: temperature dependent absorption and high-resolution fluorescence spectroscopy. *J. Phys. Chem. B* **1997**, *101*, 4448−4457.
(44) Pieper, J.; Rätsep, M.; Irrgang, K. D.; Freiberg, A. Chromophore-chromophore and chromophore-protein interactions in monomeric light-harvesting complex II of green plants studied by spectral hole burning and fluorescence line narrowing. *J. Phys. Chem. B* **2009**, *113*, 10870−10880.
(45) Hofmann, C.; Aartsma, T. J.; Michel, H.; Köhler, J. Direct observation of tiers in the energy landscape of a chromoprotein: a single-molecule study. *Proc. Natl. Acad. Sci. U. S. A.* **2003**, *100*, 15534−15538.
(46) Brecht, M.; Hussels, M.; Schlodder, E.; Karapetyan, N. V. Red antenna states of photosystem I trimers from *Arthrospira platensis* revealed by single-molecule spectroscopy. *Biochim. Biophys. Acta* **2012**, *1817*, 445−452.
(47) Hofmann, C.; Michel, H.; van Heel, M.; Köhler, J. Multivariate analysis of single-molecule spectra: surpassing spectral diffusion. *Phys. Rev. Lett.* **2005**, *94*, 195501.
(48) Hussels, M.; Brecht, M. Effect of glycerol and PVA on the conformation of photosystem I. *Biochemistry* **2011**, *50*, 3628−3637.
(49) Kern, J.; Loll, B.; Luneberg, C.; DiFiore, D.; Biesiadka, J.; Irrgang, K. D.; Zouni, A. Purification, characterisation and crystallisation of photosystem II from *Thermosynechococcus elongatus* cultivated in a new type of photobioreactor. *Biochim. Biophys. Acta* **2005**, *1706*, 147−157.
(50) Zouni, A.; Kern, J.; Frank, J.; Hellweg, T.; Behlke, J.; Saenger, W.; Irrgang, K. Size determination of cyanobacterial and higher plant photosystem II by gel permeation chromatography, light scattering, and ultracentrifugation. *Biochemistry* **2005**, *44*, 4572−4581.
(51) Hussels, M.; Konrad, A.; Brecht, M. Confocal sample-scanning microscope for single-molecule spectroscopy and microscopy with fast sample exchange at cryogenic temperatures. *Rev. Sci. Instrum.* **2012**, *83*, 123706.
(52) Bittl, R.; Schlodder, E.; Geisenheimer, I.; Lubitz, W.; Cogdell, R. J. Transient EPR and absorption studies of carotenoid triplet formation in purple bacterial antenna complexes. *J. Phys. Chem. B* **2001**, *23*, 5525−5535.
(53) Herascu, N.; Najafi, M.; Amunts, A.; Pieper, J.; Irrgang, K.-D.; Picorel, R.; Seibert, M.; Zazubovich, V. Parameters of the protein energy landscapes of several light-harvesting complexes probed via spectra hole growth kinetics measurements. *J. Phys. Chem. B* **2011**, *115*, 2737−2747.
(54) Raszewski, G.; Diner, B. A.; Schlodder, E.; Renger, T. Spectroscopic properties of reaction center pigments in photosystem II core complexes: revision of the multimer model. *Biophys. J.* **2008**, *95*, 105−119.
(55) Brecht, M.; Studier, H.; Radics, V.; Nieder, J. B.; Bittl, R. Spectral diffusion induced by proton dynamics in pigment-protein complexes. *J. Am. Chem. Soc.* **2008**, *130*, 17487−17493.
(56) Loll, B.; Kern, J.; Saenger, W.; Zouni, A.; Biesiadka, J. Towards complete cofactor arrangement in the 3.0Å resolution structure of photosystem II. *Nature* **2005**, *438*, 1040−1044.
(57) Reppert, M.; Achary, K.; Neupane, B.; Jankowiak, R. Lowest electronic states of the CP47 antenna protein complex of photosystem II: simulation of optical spectra and revised structural assignments. *J. Phys. Chem. B* **2010**, *114*, 11884−11898.
(58) Renger, T. Theory of optical spectra involving charge transfer states: dynamic localization predicts a temperature dependent optical band shift. *Phys. Rev. Lett.* **2004**, *93*, 188101.
(59) Umena, Y.; Kawakami, K.; Shen, J. R.; Kamiya, N. Crystal structure of oxygen-evolving photosystem II at a resolution of 1.9Å. *Nature* **2011**, *473*, 55−60.
(60) de Weerd, F. L.; Palacios, M. A.; Andrizhiyevskaya, E. G.; Dekker, J. P.; van Grondelle, R. Identifying the lowest electronic states of the chlorophylls in the CP47 core antenna protein of photosystem II. *Biochemistry* **2002**, *41*, 15224−15233.
(61) Müh, F.; Madjet, M. E.; Renger, T. Structure-based simulation of linear optical spectra of the CP43 core antenna of photosystem II. *Photosynth. Res.* **2012**, *111*, 87−101.
(62) Reppert, M.; Zazubovich, V.; Dang, N. C.; Seibert, M.; Jankowiak, R. Low-energy chlorophyll states in the CP43 antenna protein complex: simulation of various optical spectra. II: simulation of optical spectra and revised structural assignments. *J. Phys. Chem. B* **2008**, *112*, 9934−9947.
(63) Reddy, N.; Lyle, P. A.; Small, G. J. Application of spectral hole burning spectroscopies to antenna and reaction center complexes. *Photosynth. Res.* **1992**, *31*, 167−194.
(64) Pieper, J.; Voigt, J.; Small, G. J. Chlorophyll *a* Franck-Condon factors and excitation energy transfer. *J. Am. Chem. Soc.* **1999**, *103*, 2319−2322.
(65) Pieper, J.; Voigt, J.; Renger, G.; Small, G. J. Analysis of phonon structure in line-narrowed optical spectra. *Chem. Phys. Lett.* **1999**, *310*, 296−302.
(66) Kikas, J. Effects of inhomogenety and site selective impurity-phonon coupling in solid solutions. *Chem. Phys. Lett.* **1987**, *57*, 511−513.

DOI: 10.1021/jp510631x
J. Phys. Chem. B 2015, 119, 4203−4210